Advanced beam model for fiber-bridging in unidirectional composite double-cantilever beam specimens

András Szekrényes *, József Uj [1]

Department of Applied Mechanics, Budapest University of Technology and Economics, P.O. Box 11, H-1521 Budapest, Hungary

Abstract

This work investigates the interlaminar fracture and fiber-bridging in double-cantilever beam specimens from the theoretical and experimental points of view. Crack initiation and propagation tests were performed on unidirectional E-glass/polyester double-cantilever beam specimens. The well-known classical beam theory-based solution agrees excellently with the experimental results in the case of crack initiation tests. In contrast, the classical model seems to be inadequate for the evaluation of the propagation test data. The apparent contradiction was attributed to the fiber-bridging phenomenon. Thus, a novel beam model was developed, which accounts for the effect of fiber-bridging. Based on the solution of beam theory, the number of the bridging fibers and the bridging force can be approximated. The former reaches a peak value and decreases notably, while the force tends to a plateau value as the crack grows.
© 2005 Elsevier Ltd. All rights reserved.

1. Introduction

The double-cantilever beam (DCB) test is a standard (ASTM D5528, ISO/DIS 15024) method to measure the mode-I interlaminar fracture toughness of composite materials. Within the scope of linear elastic fracture mechanics (LEFM) the DCB specimen is treated as a slender beam. The researchers provided a large amount of theoretical analyses on the DCB specimen. An advanced solution for the DCB specimen was developed by Kanninen, applying a Timoshenko beam on Winkler-type elastic foundation [1]. Later, Williams [2] extended the elastic foundation model for orthotropic materials, the elegant solution was

---

* Corresponding author. Tel.: +36 1 463 1170; fax: +36 1 463 3471.
  E-mail addresses: szeki@mm.bme.hu (A. Szekrényes), uj@mm.bme.hu (J. Uj).
 [1] Tel.: +36 1 463 2228.

referred to by numerous authors [3–5]. In fact, the elastic foundation model does not account for the effect of fiber-bridging, which is an essential feature not only in unidirectional, but even in angle-ply laminate DCB specimens [4]. Furthermore it is observable also under mixed-mode I/II conditions [6].

The bridging fibers increase the resistance to delamination. In this case the energy release rate increases with the crack length, this feature is known as the *R*-curve effect. Numerous authors have investigated the fiber-bridging in composite materials. The phenomenon was studied by Suo et al. [7] in certain composite specimens. It was highlighted that the *R*-curve cannot be considered as a material property, since it depends on the specimen size and geometry. The concept of the bridging law is widely applied in the literature to characterize the *R*-curve for DCB specimens. Kaute et al. [8] introduced a semi-empirical model for fiber-bridging modeling. The bridging law was composed by the product of two terms: the fiber force and the number of bridging fibers per unit area of crack face. The functions of these two terms were determined based on experiments. Unfortunately this model required too much parameters to be determined. Later Yan et al. [9] introduced a numerical model based on an elastic-plastic damage interface between the adjacent plies of the composite laminate. The experiments by Hashemi et al. [10] were utilized to validate their model. Tamuzs et al. applied also the finite element technique for fiber-bridging modeling in carbon/epoxy DCB specimens [11]. The bridgings were represented by nonlinear spring elements along the bridged zone of the specimen. The behavior of the springs was controlled based on the determined bridging law. Sohn et al. investigated the fiber-bridging using the bridging stress function in the case of polycrystalline alumina composites [12]. The bridging tractions were estimated based on the measured crack opening displacement. The phenomenon was studied also in short fiber-reinforced composites. An extensive study was carried out by Lindhagen and Berglund [13], the fiber-bridging in several type of composite materials was investigated and the bridging laws were determined using the DCB coupon loaded by pure bending moments. Also, Fernberg and Berglund [14] determined the bridging law for certain short-fiber-reinforced composites. A remarkable feature is that the bridging law was found to be a material parameter in these studies.

In the present work we developed a model for fiber-bridging analysis based on classical beam theory. Traditional DCB test (see Fig. 1) including crack initiation and propagation on unidirectional E-glass/polyester specimens was performed providing input data for the analysis. The main goal of our work is to provide information on the number of bridgings and the bridging force. The approximate character of these quantities would be useful in order to understand the phenomenon more deeply. The presented method is relatively easy to apply by using a Maple worksheet.
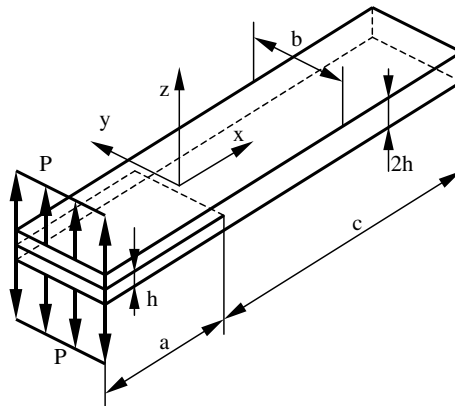

Fig. 1. DCB specimen for mode-I delamination testing.

2. Beam analysis

2.1. Analysis of the bridged DCB specimen

In this section a closed-form expression is developed for the compliance of unidirectional DCB specimens. The model incorporates the Winkler-type elastic foundation (classical solution of Williams [2]) and considers the effect of fiber-bridging. The bridgings are represented by elastic beam elements, of which extensional stiffness and initial length is utilized. Let us consider the model of the DCB specimen loaded by edge forces in Fig. 2. The governing equations are

$$\frac{d^2 w(x)}{dx^2} = \frac{-M(x)}{I_y E_{11}}, \quad -a \leqslant x \leqslant 0, \tag{1}$$

$$\frac{d^4 w(x)}{dx^4} + 4\lambda^4 w(x) = 0, \quad 0 \leqslant x \leqslant c. \tag{2}$$

The deflection functions of the lower arm can be expressed by solving Eq. (1), thus we have

$$w_{l1}(x) = -\frac{P}{I_y E_{11}} \left[\frac{1}{2} a x^2 + \frac{1}{6} x^3 \right] + c_1 x + c_2, \quad -a \leqslant x \leqslant -L_1, \tag{3}$$

$$w_{l2}(x) = -\frac{P}{I_y E_{11}} \left[\frac{1}{2} a x^2 + \frac{1}{6} x^3 \right] + \frac{P_1}{I_y E_{11}} \left[\frac{1}{2} L_1 x^2 + \frac{1}{6} x^3 \right] + c_3 x + c_4, \quad -L_1 \leqslant x \leqslant 0, \tag{4}$$

where $I_y = bh^3/12$ is the second order moment of inertia and E_{11} is the flexural modulus. The subscript 'l' refers to the lower arm. In the uncracked region the solution may be obtained by combining the generalized Krylov-functions [15], which are compiled in the Appendix A. Based on Fig. 2 the boundary and matching conditions are

$$
\begin{aligned}
&w_{l3}''(c) = 0, \quad w_{l3}'''(c) = 0, \\
&w_{l1}(-L_1) = w_{l2}(-L_1), \quad w_{l1}'(-L_1) = w_{l2}'(-L_1), \\
&w_{l2}(0) = w_{l3}(0), \quad w_{l2}'(0) = w_{l3}'(0), \\
&w_{l2}''(0) = w_{l3}''(0), \quad w_{l2}'''(0) = w_{l3}'''(0),
\end{aligned}
\tag{5}
$$

which allow the determination of the constant parameters in Eqs. (3), (4) and (A.2). For the upper half of the model the same boundary value problem may be formulated. We assume a joint-like
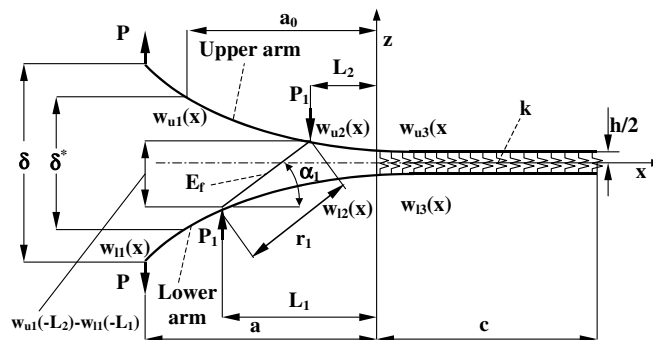

Fig. 2. For the analysis of the fiber-bridging in the DCB specimen.

connection between the bridging and the specimen arms. Thus, the elongation in the bridging is (refer to Fig. 2)

$$\Delta r_1 = r_1 - L_{01} = \sqrt{[w_{u1}(-L_2) - w_{l1}(-L_1)]^2 + L_{01}^2} - L_{01}, \tag{6}$$

where $L_{01} = |L_2 - L_1|$ is the initial length of the bridging. The displacements in Eq. (6) can be expressed by taking the deflections at the positions of $x = -L_1$ and $x = -L_2$, thus we obtain

$$w_{u1}(-L_2) = (\lambda^3[PL_2^2(3a - L_2) - 2P_1L_2^3] + 6L_2\lambda^2(Pa - P_1L_2) + 3\lambda[P(L_2 + a) - 2P_1L_2]$$
$$+ 3(P - P_1))/(6\lambda^3 I_y E_{11}), \tag{7}$$

$$w_{l1}(-L_1) = -(\lambda^3[PL_1^2(3a - L_1) - 2P_1L_1^3] + 6L_1\lambda^2(Pa - P_1L_1) + 3\lambda[P(L_1 + a) - 2P_1L_1]$$
$$+ 3(P - P_1))/(6\lambda^3 I_y E_{11}). \tag{8}$$

Eqs. (7) and (8) were substantially simplified based on the work of Ozdil and Carlsson [4]. The tensile force in the bridging can be obtained by using the following equations:

$$F_1 = s_1 \Delta r_1, \quad s_1 = \frac{A_1 E_f}{L_{01}}, \quad A_1 = n_f \frac{d_f^2 \pi}{4}, \tag{9}$$

where s_1 is the extensional stiffness, A_1 is the cross-section of the bridging, E_f is the elastic modulus of the fiber, n_f is the number of fibers per bridging and d_f is the fiber diameter. The offaxis angle between the bridging and the axis x by the help of Fig. 2 becomes

$$\alpha_1 = \arctan\left[\frac{w_{u1}(-L_2) - w_{l1}(-L_1)}{|L_2 - L_1|}\right]. \tag{10}$$

Let us denote the vertical component of the force F_1 as P_1. According to Fig. 2 P_1 may be obtained as

$$P_1 = F_1 \sin \alpha_1. \tag{11}$$

Substituting Eqs. (6)–(8) into Eq. (11) and substituting Eqs. (7) and (8) into Eq. (10) and combining it again with Eq. (11) a transcendental equation may be obtained, of which solution is the force P_1. The compliance of the lower arm becomes

$$C_1 = \frac{w_{l1}(-a)}{P}$$
$$= \left[2a^3\lambda^3 + 6a^2\lambda^2 + 6a\lambda + 3 - \frac{P_1}{P}((3aL_1^2 - L_1^3)\lambda^3 + 6aL_1\lambda^2 B + 3\lambda(L_1 + a) + 3)\right]\bigg/(6\lambda^3 I_y E_{11}). \tag{12}$$

The compliance of the DCB specimen ($C_{DCB} = \delta/P$) may be obtained by summing the compliances of the upper and lower arms, consequently we have

$$C_{DCB} = C_1 + C_u = \frac{2a^3\lambda^3 + 6a^2\lambda^2 + 6a\lambda + 3}{3\lambda^3 I_y E_{11}}$$
$$- \frac{P_1}{P} \frac{[(3a(L_1^2 + L_2^2) - (L_1^3 + L_2^3))\lambda^3 + 6a(L_1 + L_2)\lambda^2 + 3\lambda(L_1 + L_2 + 2a) + 6]}{6\lambda^3 I_y E_{11}}. \tag{13}$$

Substituting the value of λ (see Appendix A) into Eq. (13) yields:

$$C_{DCB} = C_{DCB}^0 - C_{DCB}^{FB}, \tag{14}$$

where

$$C_{\mathrm{DCB}}^0 = \frac{8a^3}{bh^3 E_{11}} \left[1 + 1.92 \left(\frac{h}{a} \right) \left(\frac{E_{11}}{E_{33}} \right)^{\frac{1}{4}} + 1.22 \left(\frac{h}{a} \right)^2 \left(\frac{E_{11}}{E_{33}} \right)^{\frac{1}{2}} + 0.39 \left(\frac{h}{a} \right)^3 \left(\frac{E_{11}}{E_{33}} \right)^{\frac{3}{4}} \right], \tag{15}$$

$$C_{\mathrm{DCB}}^{\mathrm{FB}} = \frac{P_1}{P} \frac{[(3a(L_1^2 + L_2^2) - (L_1^3 + L_2^3))\lambda^3 + 6a(L_1 + L_2)\lambda^2 + 3\lambda(L_1 + L_2 + 2a) + 6]}{6\lambda^3 I_y E_{11}}, \tag{16}$$

where the term C_{DCB}^0 is the specimen compliance based on the classical elastic foundation model [2]. The effect of fiber-bridging is incorporated in the term $C_{\mathrm{DCB}}^{\mathrm{FB}}$. The energy release rate may be obtained by using the Irwin–Kies expression [16]

$$G_{\mathrm{I}} = \frac{P^2}{2b} \frac{\mathrm{d} C_{\mathrm{DCB}}}{\mathrm{d} a}. \tag{17}$$

Using Eqs. (15) and (17) the energy release rate may be easily obtained without the bridging effect, the relevant expression [2,4,5] is not detailed here, but it will be used in the sequel. Considering Eq. (16) we must differentiate all those parameters which depend on the crack length. Although the location of the bridgings, $L_1(a)$ and $L_2(a)$ are linear functions of the crack length a, the force $P_1(a)$ as a function of the crack length is difficult to obtain [see Eqs. (10) and (11)]. Hence, a closed-from solution is not available for the energy release rate. Furthermore the dependence of L_1 and L_2 on the crack length is not considered.

2.2. Generalization for 'n' number of bridgings

It is evident, that the equations above should be generalized in order to model any amount (n) of bridging fibers. The model introduced in Section 2.1 is modified here for 'n' number of bridgings. In Fig. 3 a general asymmetric arrangement can be seen. The elongation in the 'j'th bridging is (where 'j' is a number between 1 and 'n')

$$\Delta r_j = r_j - L_{0j} = \sqrt{[w_{\mathrm{u}}(-L_{2j}) - w_{\mathrm{l}}(-L_{2j-1})]^2 + L_{0j}^2} - L_{0j}, \tag{18}$$

where $L_{0j} = |L_{2j} - L_{2j-1}|$ is the initial length of the 'j'th bridging. The value of the deflection at $x = -L_{2j}$ in the upper arm is

$$w_{\mathrm{u}}(-L_{2j}) = \sum_{i=1}^{n} (\lambda^3 [PL_{2j}^2(3a - L_{2j}) + P_i \phi_{2i}] + 6L_{2j}\lambda^2 (Pa - P_i L_{2i})$$
$$+ 3\lambda[P(L_{2j} + a) - P_i(L_{2i} + L_{2j})] + 3(P - P_i))/(6\lambda^3 I_y E_{11}), \tag{19}$$
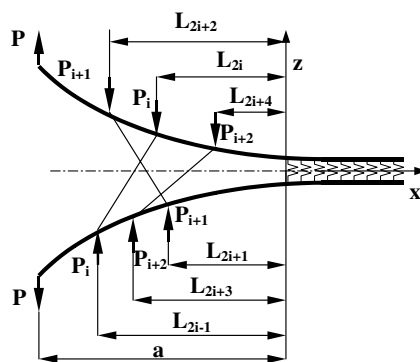

Fig. 3. A general case for asymmetrical fiber-bridging.

where

$$\phi_{2i} = L_{2i}^2(L_{2i} - 3L_{2j}), \quad \text{if } |L_{2j}| \geqslant |L_{2i}|,$$
$$\phi_{2i} = L_{2j}^2(L_{2j} - 3L_{2i}), \quad \text{if } |L_{2j}| < |L_{2i}|, \ j = 1, 2, 3, \ldots, n.$$
(20)

The deflection at the position of $x = -L_{2j-1}$ in the lower arm becomes

$$w_1(-L_{2j-1}) = -\sum_{i=1}^{n}(\lambda^3[PL_{2j-1}^2(3a - L_{2j-1}) + P_i\phi_{2i-1}] + 6L_{2j-1}\lambda^2(Pa - P_iL_{2i-1})$$
$$+ 3\lambda[P(L_{2j-1} + a) - P_i(L_{2i-1} + L_{2j-1})] + 3(P - P_i))/(6\lambda^3 I_y E_{11}),$$
(21)

where

$$\phi_{2i-1} = L_{2i-1}^2(L_{2i-1} - 3L_{2j-1}), \quad \text{if } |L_{2j-1}| \geqslant |L_{2i-1}|,$$
$$\phi_{2i-1} = L_{2j-1}^2(L_{2j-1} - 3L_{2i-1}), \quad \text{if } |L_{2j-1}| < |L_{2i-1}|, \ j = 1, 2, 3, \ldots, n.$$
(22)

It is obvious, that the distances, L_{2j} and L_{2j-1} should strictly determine the location of the '*j*'th bridging. The tensile force in the '*j*'th bridging is

$$F_j = s_j \Delta r_j, \quad s_j = \frac{A_j E_f}{L_{0j}}, \quad A_j = n_f \frac{d_f^2 \pi}{4}.$$
(23)

The offaxis angle between the '*j*'th bridging and the axis x may be obtained as

$$\alpha_j = \arctan\left[\frac{w_u(-L_{2j}) - w_1(-L_{2j-1})}{|L_{2j} - L_{2j-1}|}\right].$$
(24)

The '*j*'th force P_j according to Fig. 3 is

$$P_j = F_j \sin \alpha_j.$$
(25)

Combining Eqs. (18)–(25) the system of equations may be built, from which the solutions for the forces (P_i, $i = 1, \ldots, n$) may be obtained. The compliance of the bridged DCB specimen becomes

$$C_{\text{DCB}} = \sum_{i=1}^{n}\{\lambda^3[4Pa^3 + P_i(L_{2i}^2(L_{2i} - 3a) + L_{2i-1}^2(L_{2i-1} - 3a))] + 6\lambda^2[a(2Pa - P_i(L_{2i} + L_{2i-1}))]$$
$$+ 3\lambda[4Pa - P_i(L_{2i} + L_{2i-1} + 2a)] + 6(P - P_i)\}/(6P\lambda^3 I_y E_{11}).$$
(26)

The number of unknown forces, as well as the number of bridgings is equal to *n*. Note that interaction between elastic foundation and the bridgings is included in Eqs. (19), (21) and (26). It should be kept in mind, that the upper and lower deflection functions are forced to depend on each other in the case of asymmetrically arranged bridgings. This effect was assumed to be very small in the case of sufficient number of bridgings, and consequently, it is neglected in the above formulation. Also, the horizontal component of the tensile force in the first of Eq. (23) was ignored.

As we mentioned before, the energy release rate cannot be expressed in closed-form. In the sequel we will use only the compliance expression.

2.3. Bridging law

The *J*-integral results in the following expression for the energy release rate including the bridged zone [7,13]:

$$J = G_I = \int_0^{\delta^*} \sigma(\delta)\mathrm{d}\delta + G_{I0}, \tag{27}$$

where G_{I0} is the fracture energy from matrix cracking (and it is assumed to be a constant value), the first term is the contribution of the fiber-bridging to the steady-state fracture toughness. Differentiating Eq. (27) the bridging stress becomes

$$\sigma(\delta) = \frac{\partial G_I}{\partial \delta^*}, \tag{28}$$

where δ^* is the crack opening displacement at the initial crack tip (see Fig. 2). Eq. (28) is called the bridging law. An exact expression for the displacement at the initial tip ($\delta^* = \delta_u^* - \delta_l^*$) may be obtained by replacing L_{2j} and L_{2j-1} with $a - a_0$ in Eqs. (19)–(22).

It should be noted that the present model does not account for those bridgings, of which initial length changes (i.e. fiber peels away from matrix) as the crack propagates. Further local effects, such as fiber debonding, failure, pull-out and sliding are also ignored. All these mechanisms are demonstrated in [8]. As a consequence, the developed model is suitable only for approximate computations. Due to the complexity of our model a simple numerical solver was developed in the code Maple [17].

2.4. Crack length correction

Thamm et al. suggested a correction factor for large displacements based on a simple geometrical scheme [18]

$$a = Na^*, \quad N = 1 - \frac{1}{6}\left(\frac{\delta}{a^*}\right)^2, \tag{29}$$

where a^* is the measured, a is the corrected crack length and δ is the experimentally measured specimen displacement. The length of the initial crack was similarly corrected. Thus, the relevant equations are

$$a_0 = Na^* - N^*(a^* - a_0^*), \quad N^* = 1 - \frac{1}{6}\left(\frac{\delta^*}{a^* - a_0^*}\right)^2, \tag{30}$$

where a_0^* is the measured value of the initial crack length, a_0 is the corrected crack length and δ^* is the experimentally measured displacement at the initial crack tip (refer to Fig. 2).

3. Experiments

3.1. Data reduction

The compliance calibration (CC) method [4] was used to reduce the experimental data. The compliance of the DCB specimen may be written as

$$C = \beta a^m, \tag{31}$$

where β and m may be found by using a curve-fitting technique.

3.2. Experimental procedure

For the measurements unidirectional $[0°]_{14}$ E-glass/polyester coupons were manufactured in a special pressure block tool. The specimens have nominal width of 20 mm, thickness of $2h = 6$ mm and fiber-volume

fraction of 43%. A nylon insert with thickness of 0.04 mm was placed at the midplane of each specimen. The specimens were cut to the desired length and have been precracked in opening mode of about 4–5 mm by using a sharp blade. This involved an area full of pulled-out fibers before the crack tip, but this effect was assumed to be negligible. A millimeter scale was traced on the lateral sides of the coupons in order to facilitate the visual measurement of the crack length. The flexural modulus was determined through a three-point bending test, which resulted in $E_{11} = 33$ GPa. Additional elastic material properties were predicted by means of Niederstadt's [19] approximate rule of mixture, this way $G_{13} = 3$ GPa and $E_{33} = 7.2$ GPa was obtained. The fiber diameter and the fiber modulus is: $d_f = 12$ μm, $E_f = 70$ GPa [20], respectively.

The DCB test setup is depicted in Fig. 4. Steel hinges were bonded to the upper and lower specimen arms. The tests were performed under displacement control using an Amsler testing machine, illustrated in Fig. 4. The load/deflection data was recorded. The load values were read from the scale of the testing machine, while the deflection was monitored by the dial gauge, shown at the upper left of Fig. 4. Crack initiation/propagation was measured visually, the curved crack front was easily observable through the upper and lower specimen surfaces.

We have performed two kinds of measurements. At the first stage we eliminated the effect of fiber-bridging by using 18 specimens with the following crack lengths: 30, 35, 40, 45, 50, 55, 60, 65, 70, 75, 80, 90, 100, 110, 120, 130, 140 and 150 mm. The specimens were loaded only up to fracture initiation and the compliance was determined for each specimen at the same point. The data was fit by Eq. (31) and the energy release rate at the point of crack initiation was determined through Eq. (17). This procedure was suitable to determine the fracture properties at crack initiation without the fiber-bridging effect in a quite extended ($a = 30$–150 mm) crack length range.

At the second stage six specimens with an initial crack length of $a_0 = 30$ mm were investigated in the same test configuration, as shown in Fig. 4. In this case the complete R-curve including the bridging effect was determined within the same crack length range ($a = 30$–150 mm). The displacement at the initial crack tip was recorded by using the two dial gauges depicted in Fig. 4. It was necessary for the determination of the bridging law. The method of data reduction was the same as it was in the case of the crack initiation tests. Some specimens with extensive fiber-bridging are shown in Fig. 5.
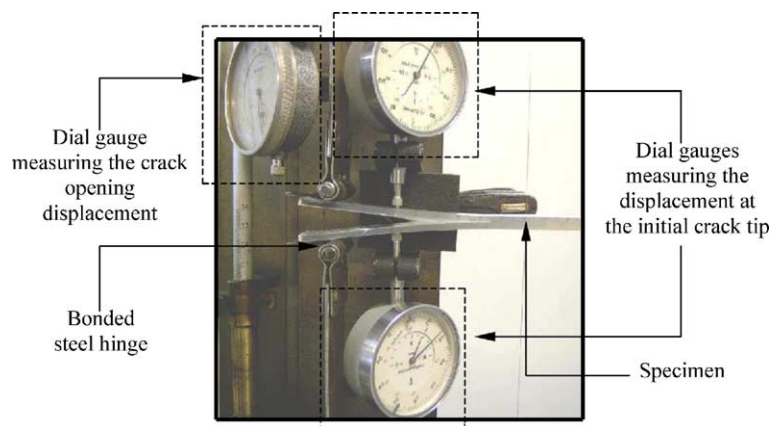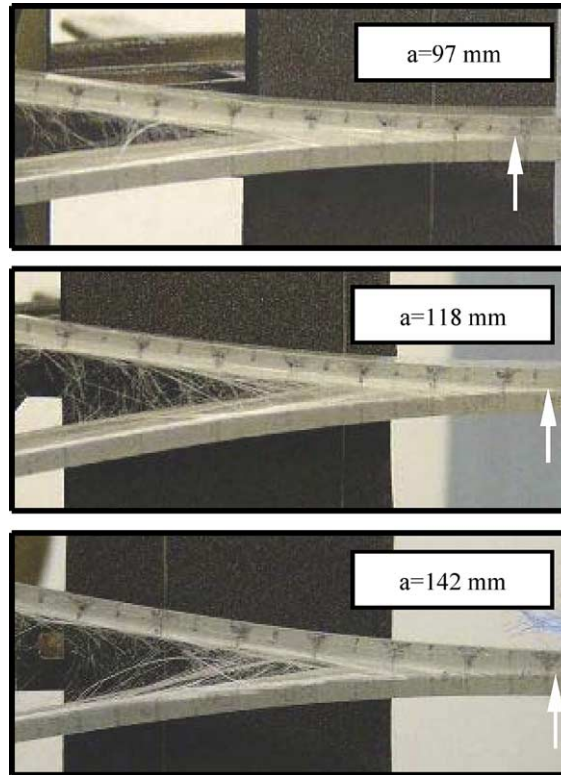

Fig. 4. Experimental setup for DCB testing.

Fig. 5. Length of the bridged zone at different crack lengths.

4. Test results

4.1. Crack initiation tests

Linear load/displacement curves were recorded through initiation tests, as shown by Fig. 6a. The compliance of the specimens versus the crack length is plotted in Fig. 6b, only Eq. (15) was used for data evaluation. The correlation was found to be excellent between the Winkler foundation model and the experimentally determined values. It is noteworthy, that the exponent (m) in Eq. (31) was less than 3. In Fig. 8b the initiation fracture resistance curve can be seen. The closed-form solution was obtained by combining Eqs. (15) and (17), of which result compared to the experimentally determined values agrees quite closely in the entire crack length interval. As a consequence, in this case the classical elastic foundation model provides the reasonably accurate description of both the compliance and the energy release rate.

4.2. Crack propagation tests

A typical load/displacement curve is plotted in Fig. 7a. The crack initiation was observed at $P = 86$–90 N, while the peak value of the load was always about 117–122 N. During the testing extensive fiber-bridging was observed as it is shown by the photographs in Fig. 5, the bridgings appeared under a shallow
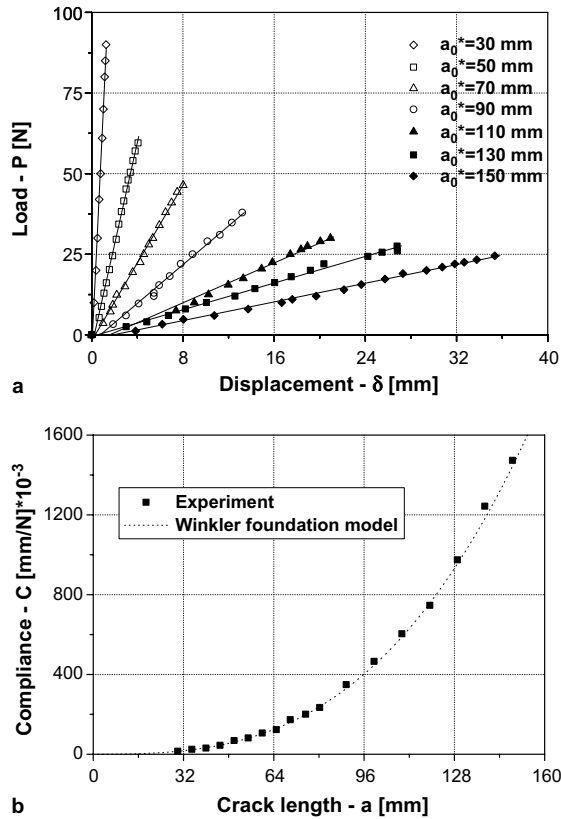
Fig. 6. Load/displacement curves (a), measured and calculated compliance (b) in the case of crack initiation tests.

angle. The crack always propagated along the midplane of the specimens. In Fig. 7b the experimental compliance values and the analytical curve [Eq. (15)] are illustrated. The exponent (m) in Eq. (31) was higher than 3 for all the six specimens. An immediate observation is that the model [Eq. (15)] significantly over-predicts the experimental compliance values. The values of the energy release rate and the averaged G_I–a data are plotted in Figs. 8a and b. Again, the closed-form solution was obtained by combining Eqs. (15) and (17). The difference was found to be particularly significant between the analytically and experimentally determined energy release rate values.

As shown by Fig. 8b, distinct initiation fracture energy values were obtained from the initiation and propagation tests at the crack length value of $a = 30$ mm. For both tests the force at crack initiation was the same (86–90 N) at this point. The difference may be explained by the fact, that the derivative of the compliance was higher in the case of crack initiation than in the case of crack propagation tests (refer to Figs. 6 and 7b).

5. Application of the developed beam model

The accuracy of the classical elastic foundation model [Eq. (15)] was proven through the initiation tests. Thus, we assume that the overpredictions experienced in the propagation tests arise due to the
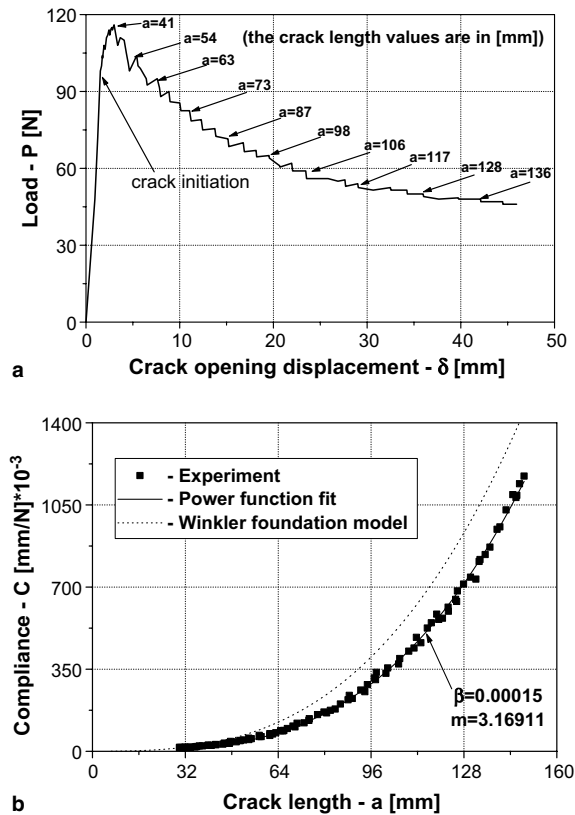
Fig. 7. Load/displacement curve (a), and compliance curves (b) in the case of crack propagation tests.

fiber-bridging phenomenon. In order to estimate the number of bridging fibers and the bridging force the experimental data was evaluated by using the model developed in Section 2.

5.1. Compliance calculation

The computation was performed according to the following procedure. Based on the propagation test data the applied load P, specimen displacements δ and δ^* measured from the tests of six specimens were averaged with respect to the crack length. The experimental compliance was calculated based on the averaged P and δ values, then the compliance values were fit by Eq. (31). The analytical compliance expression [Eq. (26)] was computed for the actual crack length. In each step the crack increment was 3–5 mm, while the number and location of the bridgings were chosen in order to hold the difference between the analytical and experimental compliance values (Fig. 7b) within ±2–3%. Also, the displacement at the initial crack tip was considered and the difference between the analytical and experimental values was held within ±2–3%. Finally, it was assumed that the average bridging stress calculated by the beam model (see Eq. (32)) is equal to that obtained by Eq. (28). Only symmetrically arranged bridgings were applied with the same fiber content. If these criterions were satisfied it was considered to be a possible solution of the problem.
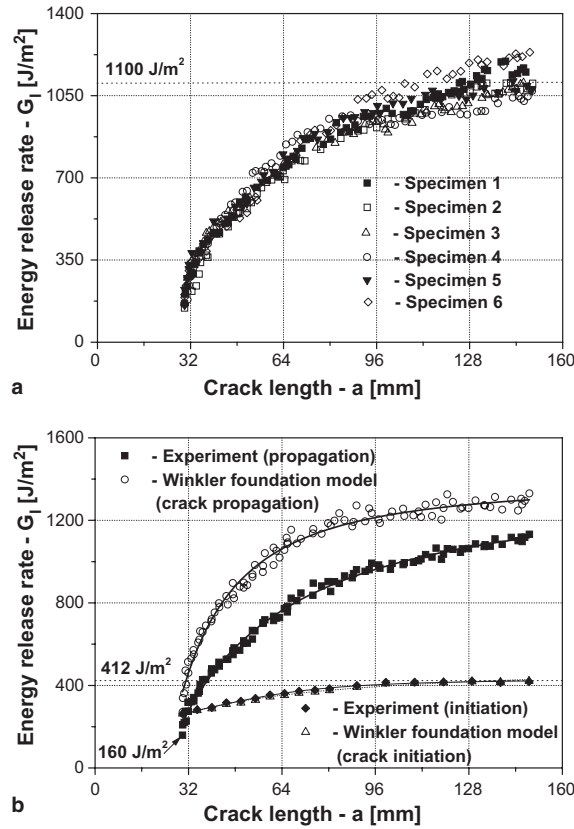
Fig. 8. G_I–a data from the propagation test of six specimens (a). R-curves at crack initiation and crack propagation (b).

5.2. Bridging law computation

Two approaches were used to calculate the nonlinear bridging law. The first method (denoted as the 'average stress' method) is based on the average bridging stress:

$$\sigma(\delta^*) = \frac{n \cdot n_{\mathrm{f}} \sum_{i=1}^{n} P_i}{A(a)}, \tag{32}$$

where n is the number of bridgings, n_{f} is the number of fibers per bridging, P_i are the forces in the bridgings and $A(a)$ is the area of the bridged zone at the actual crack length. The length of the bridged zone is illustrated in Fig. 5 at certain crack lengths, where the white arrows show the position of the crack tip. At the beginning of the delamination process the bridged zone extended over the initial crack tip with several millimeters, but it reached an approximately constant value (45 mm) during the crack propagation. The area of the bridged zone is obtained by multiplying the bridged length with the specimen width b. It should be mentioned that the bridging force is probably not uniformly distributed. Thus, the result of Eq. (32) is only approximate.

For the second approach Eq. (28) was used. Although it is based on the experimentally determined quantities, these may be calculated also by the developed beam model. The compliance values calculated from Eq. (26) may be fit by Eq. (31). The energy release rate may be obtained by using Eq. (17), then the bridging law can be determined by the help of Eq. (28). This method was denoted as the J-integral method.

Comparison of the two analytical and the experimental bridging laws is made.

6. Results and discussion

6.1. Compliance and energy release rate

The compliance values calculated by using the developed beam model are illustrated in Fig. 9a. Comparing these values with the experimental values in Fig. 7b we find that the model shows good agreement,
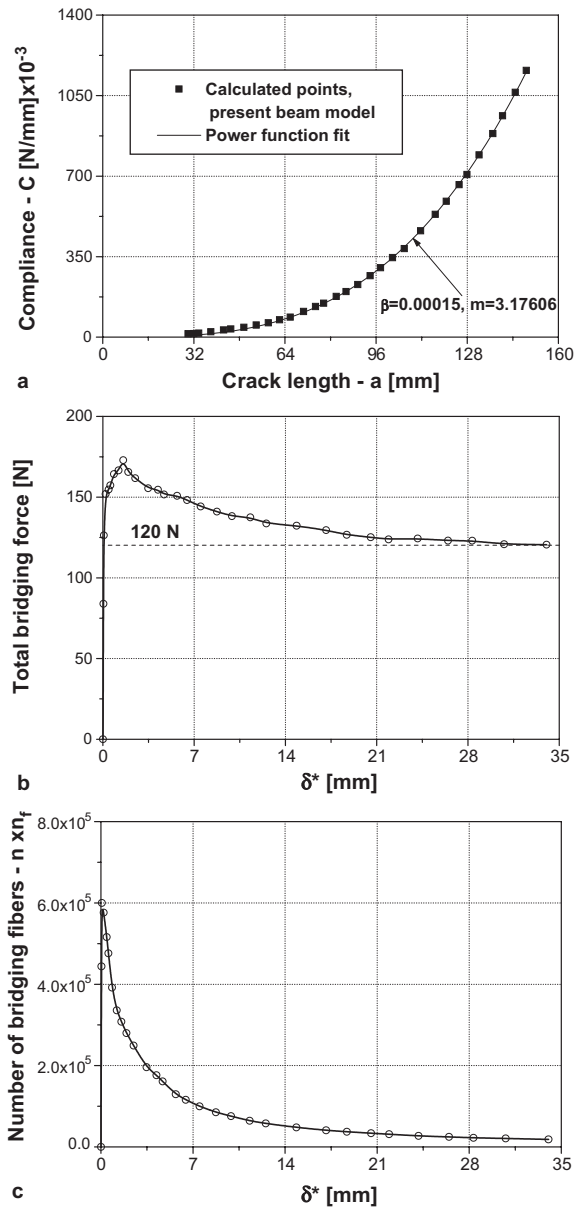

Fig. 9. Compliance calculated by the developed beam model (a). The total bridging force (b) and the total number of bridging fibers (c) against the displacement at the initial crack tip.

the mentioned deviation (2–3%) is not perceptible. The coefficient (β) and the exponent (m) of the fit curves [Eq. (31)] are essentially the same in Fig. 7b and in Fig. 9a. As a consequence, the same energy release rate values may be determined from the calculated compliance curve in Fig. 9a, as those plotted in Fig. 8b.

6.2. Bridging force and number of bridging fibers

The total bridging force and the number of bridging fibers are illustrated in Figs. 9b and c as a function of the displacement at the initial tip. The force reaches a peak value of about 176 N and then it slightly decreases until the value of 120 N. At the beginning of the delamination the number of bridging fibers reaches a maximum value and then it decreases significantly as the crack opens (Fig. 9c). Kaute et al. [8] presented quite similar results. In their work the fiber force was assumed to be constant after crack initiation, while the number of bridgings decreased in accordance with an exponential function.

6.3. Bridging law

Fig. 10a shows the G_I–δ^* curves determined from experiment and analysis. As expected, the correlation was found to be excellent, despite the beam model shows a little overestimation. Figs. 10b and c demonstrate the bridging laws. The result of the average stress method [Eq. (32)] is depicted in Fig. 10c, in comparison with the J-integral approach the agreement seems to be very good. According to the average stress method the stress is equal to zero at crack initiation, it reaches a peak value (0.32 MPa, refer to Fig. 10c) and finally decays notably. At crack initiation the J-integral method indicates 4.92 MPa value based on beam analysis and 3.94 MPa from experiment (Fig. 10b). For comparison the work by Tamuzs et al. [11] may be referred to, wherein the presented bridging law follows the same trend as found by us.

6.4. Matrix cracking and fiber-bridging

According to Eq. (27) the term G_{I0} from matrix cracking is assumed to be a constant value. The first term in Eq. (27) is defined by the integral over the total crack opening. Consequently, the term, G_{I0} may be determined by subtracting the first term from the total energy release rate. This may be done if the fit curves in Fig. 10a are known. Based on the experimentally determined bridging law this term is approximately equal to 160 J/m^2, which is identical to the initiation value in Fig. 8b. A reasonable assumption is, that during crack initiation tests the total energy release rate comes from matrix cracking, and it is a constant value at any crack length. In spite of this the initiation toughness increases (from 280 to 415 J/m^2) with the crack length (see Fig. 8b). Hashemi et al. [10] experienced similar behavior to that found by us. In fact the dependence of the initiation energy release rate on the initial crack length is not serious in Fig. 8b and we assumed that for the current material Eq. (26) is valid.

It was mentioned by Lindhagen and Berglund [13] that as the crack advances the steady-state toughness is equal to the area under the curve of the bridging law. Note that the length of the specimen was not large enough to reach a plateau value, in other words some fiber-bridging was observed at the end of the delamination process (refer to Fig. 8b). Lindhagen and Berglund investigated short-fiber-reinforced composite specimens and they have found that in some cases the fracture energy from matrix cracking may be neglected. On the base of our experiments the fracture toughness increases up to 1100 J/m^2. At this point the matrix cracking (160 J/m^2) contributes to the total fracture energy with about 15%, which is not negligible.
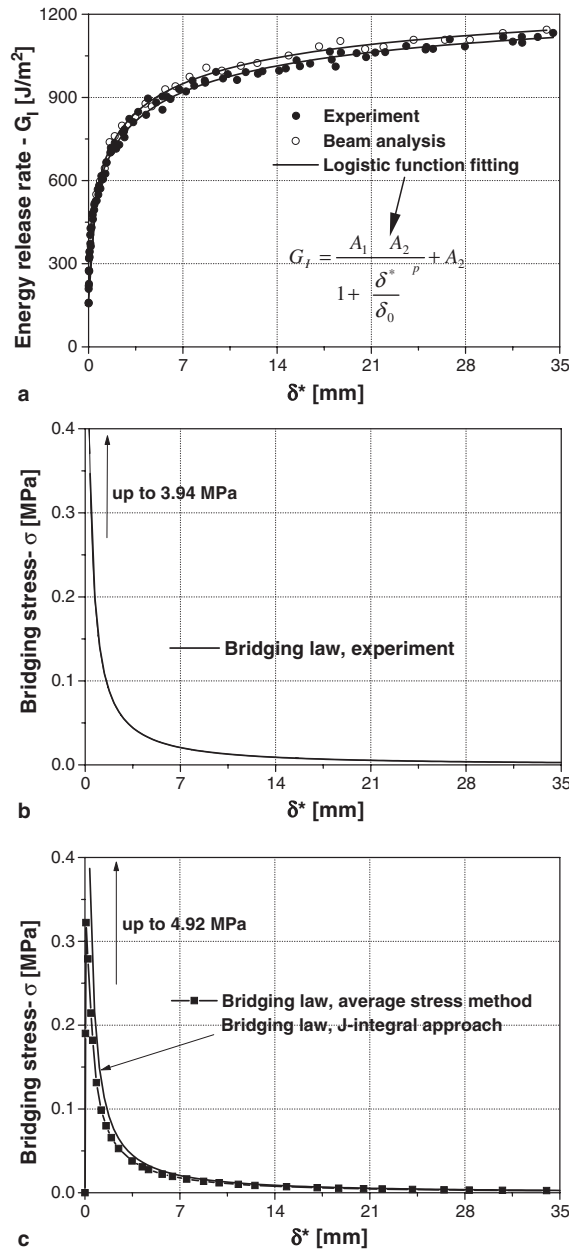
Fig. 10. G_I–δ^* curves from experiment and beam analysis (a). Experimental bridging law (b). Analytical bridging law from average stress and J-integral approach (c).

7. Conclusions

The fiber-bridging phenomenon was investigated using linear beam theory and experiments in unidirectional E-glass/polyester DCB coupons. Extensive fiber-bridging was observed during the crack propagation tests. The objective of the present work was to determine approximately the number of bridging fibers and

the bridging force. Based on linear beam theory the compliance of the bridged DCB specimen was derived. The bridging mechanism was simulated by elastic beam elements. Applying the developed model a hyperbolic character was found in the case of the number of bridging fibers as a function of the displacement at the initial crack tip. The bridging force reaches a peak value first, and then it tends to a plateau value of about 120 N as the crack advances. The bridging law was calculated based on experiments and analysis. Comparison between them showed good agreement, but it should be kept in mind that in one of the analytical approaches the average bridging stress was considered.

The obtained results were compared with other ones, previously published on similar systems. Similar behavior was found, which partly confirms the analytical solution. From other perspectives the present formulation involves several approximations. For instance, local effects (fiber pull-out, fiber breakage, etc.) were not taken into account.

Although the application of the developed model is slightly time-consuming, the calculation may be performed by the help of few additional properties, namely the fiber diameter d_f and the elastic modulus of the fibers E_f.

Acknowledgements

Appendix A

The homogeneous, generalized Krylov-functions are [15]

$$V_1(x) = \cosh(\lambda x)\cos(\lambda x), \tag{A.1}$$

$$V_2(x) = \frac{1}{2}[\cosh(\lambda x)\sin(\lambda x) + \sinh(\lambda x)\cos(\lambda x)],$$

$$V_3(x) = \frac{1}{2}\sinh(\lambda x)\sin(\lambda x),$$

$$V_4(x) = \frac{1}{4}[\cosh(\lambda x)\sin(\lambda x) - \sinh(\lambda x)\cos(\lambda x)].$$

The deflection function of the uncracked region is

$$w_{13}(x) = c_5 \cdot V_1(x) + c_6 \cdot V_2(x) + c_7 \cdot V_3(x) + c_8 \cdot V_4(x), \quad 0 \leqslant x \leqslant c, \tag{A.2}$$

where according to [4]:

$$\lambda = \frac{6^{1/4}}{h}\left(\frac{E_{33}}{E_{11}}\right)^{1/4}, \tag{A.3}$$

where E_{33} is the through-thickness modulus of the specimen.

References

[1] Kanninen MF, Popelar CH. Advanced fracture mechanics. New York: Oxford University Press; 1985.
[2] Williams JG. End corrections for orthotropic DCB specimens. Compos Sci Technol 1989;35:367–76.

[3] Li Z. A new technique for determining fracture toughness K_{Ic} and its confidence with single DCB specimen. Engng Fract Mech 1996;55:133–7.

[4] Ozdil F, Carlsson LA. Beam analysis of angle-ply laminate DCB specimens. Compos Sci Technol 1999;59:305–15.

[5] Olsson R. A simplified improved beam analysis of the DCB specimen. Compos Sci Technol 1992;43:329–38.

[6] Ivens J, Albertsen H, Wevers M, Verpoest I, Peters P. Interlaminar fracture toughness of CFRP influenced by fiber surface treatment: Part 2. Modeling of the interface effect. Compos Sci Technol 1995;54:133–45.

[7] Suo Z, Bao G, Fan B. Delamination *R*-curve phenomena due to damage. J Mech Phys Solids 1992;40:1–16.

[8] Kaute DAW, Shercliff HR, Ashby MF. Modelling of fibre bridging and toughness of ceramic matrix composites. Scripta Metall Mater 1995;32:1055–60.

[9] Yan A-M, Marechal E, Nguyen-Dang H. A finite element model of mixed-mode delamination in laminated composites with an *R*-curve effect. Compos Sci Technol 2001;61:1413–27.

[10] Hashemi S, Kinloch J, Williams JG. Mechanics and mechanisms of delamination in a poly(ether sulphone)-fibre composites. Compos Sci Technol 1990;37:429–62.

[11] Tamuzs V, Tarasovs S, Vilks U. Progressive delamination and fiber bridging modelling in double cantilever beam composite specimen. Engng Fract Mech 2001;68:513–25.

[12] Sohn K-S, Lee S, Baik S. Analysis of bridging stress effect of polycrystalline alumina using double cantilever beam method. Acta Mater 1997;45:3445–57.

[13] Lindhagen JE, Berglund LA. Application of bridging-law concepts to short-fibre composites. Part 1: DCB test procedures for bridging law and fracture energy. Compos Sci Technol 2000;60:871–83.

[14] Fernberg SO, Berglund LA. Bridging law and toughness characterization of CSM and SMC composites. Compos Sci Technol 2001;61:2445–54.

[15] Ponomarjov SD. Strength calculations in mechanical engineering. Beams and springs, vol. 2. Budapest: Technical Book Publisher; 1964 [in Hungarian].

[16] Broek D. Elementary engineering fracture mechanics. The Hague: Martinus Nijhoff Publishers; 1982.

[17] Heck A. Introduction to maple. New York: Springer-Verlag; 1993.

[18] Thamm F, Borbás L, Gáti R, Gál J. Interlaminar fracture toughness of native composite laminates. Plastics and Rubber 1996;33:246–50 [in Hungarian].

[19] Thamm F. Strength of plastic materials II. Budapest: Technical Book Publisher; 1985 [in Hungarian].

[20] Phillips LN. Design with advanced composite materials. London: The Design Council, Springer-Verlag; 1989.